Combined Raman scattering and *ab initio* investigation of pressure-induced structural phase transitions in the scintillator $ZnWO_4$

D. Errandonea,[1,*] F. J. Manjón,[2] N. Garro,[3] P. Rodríguez-Hernández,[4] S. Radescu,[4] A. Mujica,[4] A. Muñoz,[4] and C. Y. Tu[5]
[1]*MALTA Consolider Team, Fundacion General de la Universidad de Valencia-ICMUV, Universitat de València, Edificio de Investigación, c/Dr. Moliner 50, 46100 Burjassot, Valencia, Spain*
[2]*MALTA Consolider Team, Departamento de Física Aplicada-IDF, Universitat Politècnica de València, 46022 València, Spain*
[3]*Fundació General de la Universitat de València-ICMUV, Universitat de València, Polígon La Coma s/n, 46980 Paterna, Spain*
[4]*MALTA Consolider Team, Departamento de Física Fundamental II, Universidad de La Laguna, La Laguna, 38205 Tenerife, Spain*
[5]*Fujian Institute of Research on the Structure of Matter, Chinese Academy of Sciences, Fuzhou, Fujian 350002, China and Graduate School of Chinese Academy of Sciences, Beijing 100039, China*
(Received 9 April 2008; published 20 August 2008)

The room-temperature Raman scattering was measured in $ZnWO_4$ up to 45 GPa. We report the pressure dependence of all the Raman-active phonons of the low-pressure wolframite phase. As pressure increases additional Raman peaks appear at 30.6 GPa due to the onset of a reversible structural phase transition to a distorted monoclinic β-fergusonite-type phase. The low-pressure and high-pressure phases coexist from 30.6 to 36.5 GPa. In addition to the Raman measurements we also report *ab initio* total-energy and lattice-dynamics calculations for the two phases. These calculations helped us to determine the crystalline structure of the high-pressure phase and to assign the observed Raman modes in both the wolframite and β-fergusonite phases. Based upon the *ab initio* calculations we propose the occurrence of a second phase transition at 57.6 GPa from the β-fergusonite phase to an orthorhombic *Cmca* phase. The pressure evolution of the lattice parameters and the atomic positions of wolframite $ZnWO_4$ are also theoretically calculated, and an equation of state reported.

DOI: 10.1103/PhysRevB.78.054116 PACS number(s): 62.50.−p, 63.20.−e, 78.30.−j

I. INTRODUCTION

Materials belonging to the tungstate family (AWO_4) have a long history of practical application, having already been used by Edison[1] in 1896 to detect x-rays. As a consequence of their technological importance; AWO_4 compounds have been the object of extensive research. The interest in them arises from their optical properties, which form the basis of their wide application as phosphors, laser crystals, and scintillation detectors.[2–4] Recently, new applications for these materials have emerged, including large volume scintillators for high-energy physics[5] and detectors devoted to the search of rare events (e.g., interactions with weakly interactive massive particles).[6] In particular, zinc tungstate ($ZnWO_4$), also known by its mineral name sanmartinite, is a wide gap semiconductor with band-gap energy close to 4 eV (Ref. 7) and is a promising material for the new generation of radiation detectors.[8]

It is well known that AWO_4 compounds mostly crystallize either in the tetragonal scheelite [space group (SG): $I4_1/a$, with $Z=4$] or in the monoclinic wolframite (SG: $P2/c$, with $Z=2$) structures depending on the size of the countercation A.[9] In particular, $ZnWO_4$ has a wolframite-type crystalline structure [see Fig. 1(a)],[10] with two formula units (Z) per crystallographic cell. In this structure, both Zn and W cations have octahedral oxygen coordination and each octahedron shares two corners with its neighbors. In particular, the WO_6 octahedra are highly distorted since two of the W-O distances are much larger than the other four distances.

High-pressure research has proved to be an efficient tool to improve the understanding of the main physical properties of AWO_4 compounds. Although there is abundant literature on high-pressure studies in these materials, much of the research has been carried out on scheelite structured compounds such as $CaWO_4$, $SrWO_4$, $BaWO_4$, and $PbWO_4$.[11–24] These studies have been recently reviewed[25] and have established that all the members of the scheelite subfamily of tungstates undergo a sequence of pressure driven structural phase transitions with space-group changes $I4_1/a \rightarrow I2/a \rightarrow P2_1/n$, in good agreement with the conclusions drawn from the application of the Bastide diagram[26] to ABO_4 compounds.[23,25] Additionally, optical-absorption measurements on $PbWO_4$ (Ref. 27) and luminescence studies on $SrWO_4$ (Refs. 28 and 29) showed that the electronic structure of scheelite tungstates is also strongly affected by pressure.

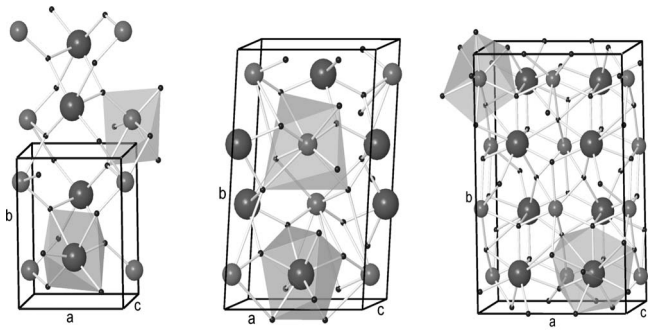

FIG. 1. (a) Perspective drawing of the crystal structure of wolframite $ZnWO_4$, (b) perspective drawing of the crystal structure of the proposed β-fergusonite phase of $ZnWO_4$, and (c) perspective drawing of the crystal structure of proposed *Cmca* phase of $ZnWO_4$. Large circles: Zn; medium circles: W; and small circles: O. The conventional unit cell is represented with solid lines. W-O and Zn-O bonds are also shown as well as the different polyhedra.

TABLE I. Experimental and calculated crystal parameters of wolframite $ZnWO_4$. Space group $P2/c$, with $Z=2$. Calculated parameters are given at different pressures.

	Neutron-diffraction[a] ambient pressure	X-ray diffraction (this work) ambient pressure	*Ab initio* calculations (this work) ambient pressure	*Ab initio* calculations (this work) $P=27.2$ GPa
a	4.693 Å	4.680 Å	4.741 Å	4.516 Å
b	5.721 Å	5.712 Å	5.824 Å	5.521 Å
c	4.928 Å	4.933 Å	4.977 Å	4.799 Å
β	90.632°	90.3°	90.759°	89.899°
Zn site: $2f$	$x=0.5$	$x=0.5$	$x=0.5$	$x=0.5$
	$y=0.6833$	$y=0.697$	$y=0.6811$	$y=0.6780$
	$z=0.25$	$z=0.25$	$z=0.25$	$z=0.25$
W site: $2e$	$x=0$	$x=0$	$x=0$	$x=0$
	$y=0.1823$	$y=0.178$	$y=0.1813$	$y=0.1873$
	$z=0.25$	$z=0.25$	$z=0.25$	$z=0.25$
O_1 site: $4g$	$x=0.2547$	$x=0.244$	$x=0.2561$	$x=0.2570$
	$y=0.3772$	$y=0.372$	$y=0.3741$	$y=0.3908$
	$z=0.4005$	$z=0.394$	$z=0.4025$	$z=0.4101$
O_2 site: $4g$	$x=0.2171$	$x=0.203$	$x=0.2153$	$x=0.2292$
	$y=0.8955$	$y=0.904$	$y=0.8943$	$y=0.9009$
	$z=0.4360$	$z=0.456$	$z=0.4365$	$z=0.4348$

[a]Reference 34.

Given the structural differences between wolframite and scheelite,[9] their structures are expected to be modified in a different way upon compression.[30] However, very little information currently exists on how the crystal structures of $ZnWO_4$ and isostructural tungstates (e.g., $CdWO_4$ and $NiWO_4$) are affected by pressure. Only a couple of works reporting Raman measurements under pressure in $CdWO_4$ up to 40 GPa (Ref. 31) and in $ZnWO_4$ up to 24 GPa (Ref. 32) were performed. Some contradictions and many unanswered questions arise from the information reported in these two works. For example, $ZnWO_4$ was found to remain stable in the wolframite structure up to 24 GPa,[32] while two phase transitions were reported in $CdWO_4$ at 10 and 20 GPa.[31] In order to improve the knowledge of the physical properties of wolframite-type tungstates, as part of our project to study the structural stability of orthotungstates, we have carried out Raman spectroscopy measurements on $ZnWO_4$ up to 45 GPa. The obtained results are interpreted on the basis of first-principles total-energy and lattice dynamics calculations. The technical aspects of the experiments and calculations are described in Secs. II and III. The results are presented and discussed in Sec. IV. Finally, we present the conclusions of this work in Sec. V.

II. EXPERIMENT DETAILS

The samples used in the present experiments were obtained from a wolframite-type $ZnWO_4$ single crystal grown by the Czochralski method.[33] In order to get a high-quality crystal of $ZnWO_4$, the used raw materials such as ZnO and WO_3 must be of high purity. The raw materials used were ZnO (99.9%) and WO_3 (99.9%). The initial compounds were mixed in a carnelian bowl and sintered for almost three days at 1320 K. Then the charge was deposited in a Pt crucible bowl of $\varnothing 55\times 30$ mm^2 and placed in a DJL-400 furnace. With the Pt wire rotating at a rate of 12 rpm and a pulling rate of 1.2 mm/h, the crystal was grown. When the procedure was over, the crystal was drawn out and cooled down at room temperature (RT) at a rate of 10–30 °C/h. The obtained crystal was optically transparent and color free. X-ray diffraction measurements at ambient conditions showed that its diffraction pattern was in agreement with that of sanmartinite. The refined unit-cell parameters ($a=4.680$ Å, $b=5.712$ Å, $c=4.933$ Å, and $\beta=90.3°$) and atomic positions compare well with earlier reported data from neutron powder diffraction[34] (see Table I).

Two different samples were used for our Raman measurements under pressure. Sample 1 was a 10-μm-thick plate cleaved along the {010} plane[35] from a $ZnWO_4$ single crystal. It was pressurized up to 21 GPa with a 16:3:1 methanol-ethanol-water mixture as its pressure transmitting medium. Sample 2 consisted in a prepressed pellet prepared using a finely ground powder obtained from the single crystal of $ZnWO_4$. It was pressurized up to 45 GPa with argon (Ar) to ensure better quasihydrostatic conditions.[36,37] The pressure was determined by the ruby fluorescence technique[38] using the pressure scale recalibrated by Dewaele *et al.*[39] The RT Raman experiments were performed in backscattering geometry using the 488-nm (2.54 eV) line of an Ar^+-ion laser with a power of less than 100 mW before the diamond-anvil cell (DAC) to avoid sample heating. Laser heating of the sample is negligible in the whole pressure range covered by our experiments because the laser energy is always below the band gap of $ZnWO_4$ in both the low-pressure and high-pressure phases. Note that in wolframite $ZnWO_4$ the band

gap is E_g=4 eV (Ref. 7) and its pressure coefficient is positive (dE_g/dP=10 meV/GPa),[40] and that E_g is not expected to close more than 1 eV at the pressure-induced phase transition.[27] A Mitutoyo 20× long working distance objective was employed for focusing the laser on the sample and for collecting the Raman spectra. The dispersed light was analyzed with a Jobin-Yvon T64000 triple spectrometer equipped with a confocal microscope in combination with a liquid nitrogen cooled multichannel charge coupled device (CCD) detector. The spectral resolution was better than 1 cm^{-1}, and Ar and He plasma lines were used to calibrate the Raman and photoluminescence spectra.

III. CALCULATION TECHNIQUE

Total-energy calculations and lattice dynamics calculations were done within the framework of the density-functional theory (DFT) and the pseudopotential method using the Vienna *ab initio* simulation package (VASP), of which a detailed account can be found in Ref. 41 and references therein. The exchange and correlation energy was initially taken in the generalized gradient approximation (GGA) according to Perdew-Burke-Ernzerhof[42] (PBE) prescription. The projector augmented wave (PAW) scheme[43] was adopted and the semicore 5*p* electrons of W were dealt with explicitly in the calculations. The set of plane waves used extended up to a kinetic-energy cutoff of 500 eV. This large cutoff was required to deal with the O atoms within the PAW scheme to ensure highly converged results. The Monkhorst-Pack grid used for Brillouin-zone integrations ensured highly converged results (to about 1 meV per formula unit). We use the 24 *k*, 26 *k*, 22 *k*, and 6 *k* points to study the wolframite, $CuWO_4$-type, β-fergusonite, and *Cmca* structures, respectively. At each selected volume, the structures were fully relaxed to their equilibrium configuration through the calculation of the forces on atoms and the stress tensor—see Ref. 19. In the relaxed equilibrium configuration, the forces are less than 0.002 eV/A and the deviation of the stress tensor from a diagonal hydrostatic form is less than 1 kbar (0.1 GPa). The highly converged results on forces are required for the calculation of the dynamical matrix using the direct force constant approach (or supercell method).[44] The construction of the dynamical matrix at the Γ point is particularly simple and involves separate calculations of the forces in which a fixed displacement from the equilibrium configuration of the atoms within the *primitive* unit cell is considered. Symmetry aids by reducing the number of such independent distortions and by reducing the amount of computational effort in the study of the analyzed structures considered in our work. Diagonalization of the dynamical matrix provides both the frequencies of the normal modes and their polarization vectors. It allows us to identify the irreducible representation and the character of the phonon modes at the zone center.

IV. RESULTS AND DISCUSSION

A. Raman measurements of the low-pressure phase

A group theoretical analysis of the wolframite structure of $ZnWO_4$ yields 36 lattice modes at the Γ point: $8A_g+10B_g+8A_u+10B_u$, with the 18 even (*g*) vibrations being Raman-active modes, $8A_g+10B_g$. Symmetry assignments of the modes in the wolframite structure was previously made for all the 18 phonons by applying polarization selection rules in $ZnWO_4$.[32,45,46] The symmetry assignments reported in Ref. 46 are shown in Table II and have been confirmed by our *ab initio* calculations, as we will discuss latter. In scheelite-type AWO_4 compounds it has been proved that one can distinguish two types of vibrational modes: internal and external modes with respect to the WO_4 tetrahedra. The internal modes correspond to normal motions of atoms inside the WO_4 tetrahedra, while the external modes involve motions of WO_4 tetrahedra against the A atom. It is expected that the phonon frequencies of the internal modes will be higher than those of the external modes because the internal covalent bonding within the WO_4 tetrahedra is stronger than the external lattice binding. Due to the incompressibility of the WO_4 tetrahedra, it is also expected that the Grüneisen parameters of the internal modes were smaller than those of the external modes. Out of the internal modes, there are four stretching modes arising from each of the four W-O bonds in the WO_4 tetrahedra. A similar reasoning can be applied to AWO_4 wolframites assuming the incompressibility of WO_6 octahedra with respect to the ZnO_6 octahedra. Therefore, one would expect six internal stretching modes arising from each of the six W-O bonds in the WO_6 octahedra. These six internal stretching modes have been assigned in the literature by means of pressure and temperature dependent Raman studies and by comparison with other compounds.[32,45,46] However, there are important contradictions among different authors on this assignment.

Figure 2 shows the RT Raman spectra of sanmartinite measured in sample 2 at selected pressures up to 40.2 GPa. The Raman spectra should correspond to a mixture of polarizations because of the use of a powder sample. In Fig. 2, it can be seen that up to 33.3 GPa it is possible to clearly distinguish the 18 Raman modes of wolframite $ZnWO_4$. Table II summarizes the phonon frequencies we measured at ambient pressure (0.0001 GPa) and compared them with those reported in the literature and those we calculated using *ab initio* lattice dynamics. The agreement between our results and those previously published[32,45,46] is quite good. Table II also summarizes the pressure coefficients ($d\omega/dP$) of the Raman modes of sanmartinite and their Grüneisen parameters ($\gamma=B_0/\omega\cdot d\omega/dP$, where B_0 is the bulk modulus). Figure 3 shows the pressure evolution of the wolframite phonons extracted from the two different samples we studied. Results obtained from the two samples agree very well among themselves. From our experiments we determine slightly different pressure dependences for the Raman phonons than that of Perakis *et al.*[32] In fact, for three phonons (A_g mode near 342 cm^{-1}, B_g mode near 313 cm^{-1}, and B_g mode near 190 cm^{-1}) our pressure coefficients almost doubled the values previously reported (see Table II). At present we have no explanation for the observed differences in the pressure coefficients between the two high-pressure works. However, the fact that our *ab initio* calculations are in much better agreement with our measurements (see Table II) gives additional support to the accuracy of our measurements.

TABLE II. *Ab initio* calculated and experimental zero pressure frequencies, pressure coefficients, and Grüneisen parameters of the Raman modes in wolframite $ZnWO_4$. The asterisks indicate the internal stretching modes. The Grüneisen parameter has been calculated using the calculated bulk modulus $B_0=140$ GPa as indicated in the text.

Mode	Experiment[a]			Experiment[b]		Theory[a]	
	ω (cm^{-1})	$d\omega/dP$ (cm^{-1}/GPa)	γ	ω (cm^{-1})	$d\omega/dP$ (cm^{-1}/GPa)	ω (cm^{-1})	$d\omega/dP$ (cm^{-1}/GPa)
B_g	91.5	0.95	1.45	91	1.3	83.7	1.02
A_g	123.1	0.65	0.74	123	1.1	118.6	0.48
B_g	145.8	1.2	1.15	145.5	2.05	137.2	1.33
B_g	164.1	0.72	0.61	163.5	0.85	163.3	0.42
B_g	189.6	0.67	0.49	189.5	0.32	182.2	0.41
A_g	196.1	2.25	1.61	195	3.3	185.7	2.52
B_g	267.1	1.32	0.69	266	1.25	261.2	2.16
A_g	276.1	0.87	0.44	274	0.88	263.7	0.82
B_g	313.1	1.74	0.78	314.5	1	298.3	1.44
A_g	342.1	1.74	0.71	341.5	0.85	324.2	1.7
B_g	354.1	3.87	1.53	355	4.6	342.1	3.3
A_g*	407	1.65	0.57	407.5	1.4	383.8	1.84
B_g	514.5	3.18	0.86	515.5	3.3	481.1	3.1
A_g*	545.5	3	0.77	545	3.4	515.4	3.07
B_g*	677.8	3.9	0.80	677	3.9	635.5	3.9
A_g*	708.9	3.3	0.65	708.5	3.3	678.5	3.24
B_g*	786.1	4.4	0.78	787	4.8	753.3	4.0
A_g*	906.9	3.7	0.57	906	4.1	861.8	3.36

[a]This work.
[b]Reference 32.

In order to calculate the mode Grüneisen parameters in wolframite $ZnWO_4$ its bulk modulus at zero pressure is needed. Since this magnitude has not been experimentally determined yet, we used the value we obtained from our *ab initio* calculations ($B_0=140$ GPa) to calculate the mode Grüneisen parameters reported in Table II. The bulk modulus of AWO_4 wolframite tungstates can be also estimated from the cation formal charge of the element A and the mean A-O distance using the empirical law reported in Ref. 17. This law was originally established for ABX_4 compounds with the scheelite, zircon, or similar structures—in which the BX_4 tetrahedral units have a very low polyhedral compressibility. However, as the first approximation, the same law can also be applied to wolframite compounds since in these compounds the WO_6 octahedra are significantly less compressible than the AO_6 octahedral.[47] Within this framework, we obtain for $ZnWO_4$, $B_0=130\pm8$ GPa and for $CdWO_4$ $B_0=120\pm8$ GPa. The second value is in good agreement with the bulk modulus obtained from the low-pressure data reported by Macavei and Schulz,[47] confirming the predictive capability of the model developed by Errandonea *et al.*[17] The obtained bulk modulus for $ZnWO_4$ (130 GPa) is close to our theoretical calculations (140 GPa).

In a first attempt to identify the six internal stretching modes of the W-O atoms in the distorted WO_6 octahedra of $ZnWO_4$, Liu *et al.*[45] assigned them to the modes at 906, 787, and 407 cm^{-1} on the basis of the bond lengths and Raman frequencies in the WO_6 group. Afterwards, Wang *et al.*[46] assigned the internal stretching modes to the phonons observed near 906, 787, 709, 407, 342, and 190 cm^{-1} on the basis of the temperature dependence of the Raman frequencies. However, this assignment is in contradiction with the fact that the frequencies of the internal modes are expected to be higher than those of the external modes. These authors argue in favor of their assignment that the oxygen sharing between WO_6 and ZnO_6 octahedra may cause a considerable overlap in the frequency range for the two types of vibrations. This overlapping between internal and external modes was already discussed in scheelite tungstates and molybdates by Tarte and Liegeois-Duyckaerts,[48,49] who claimed that no clear distinction can be made between internal and external modes. More recently, Perakis *et al.*[32] corrected the previous assignment (based upon high-pressure Raman spectroscopy measurements) for the internal stretching modes including the phonon at 677 cm^{-1} but not the phonon at 190 cm^{-1}. Our measurements and calculations support this correction. However we also suggest that the A_g phonon at 545 cm^{-1} is an internal stretching mode in contrast to the A_g phonon at 342 cm^{-1} previously proposed. The assignment of the internal stretching modes can be seen in Table II. It is worth commenting here that after the assignment we proposed for the internal stretching modes they consist of the four A_g modes and the two B_g modes with the highest frequencies, which is in full agreement with the idea that in AWO_4 com-

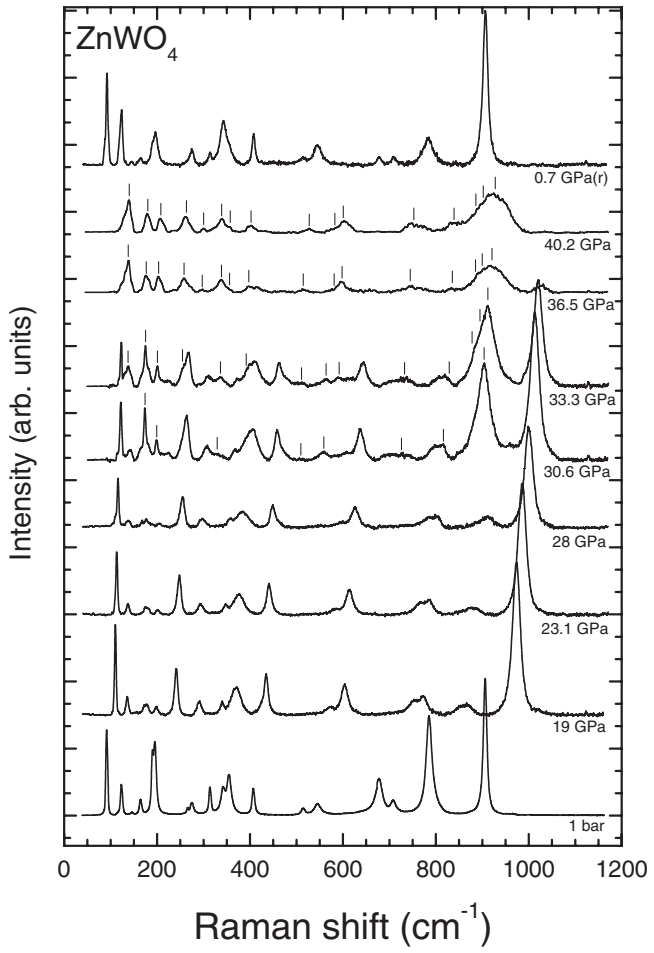

FIG. 2. Raman spectra of wolframite $ZnWO_4$ at different pressures. Ticks indicate the position of the Raman peaks assigned to the high-pressure phase. All of the spectra were measured on pressure increase with the exception of the spectra marked with (*r*), which was taken after pressure release.

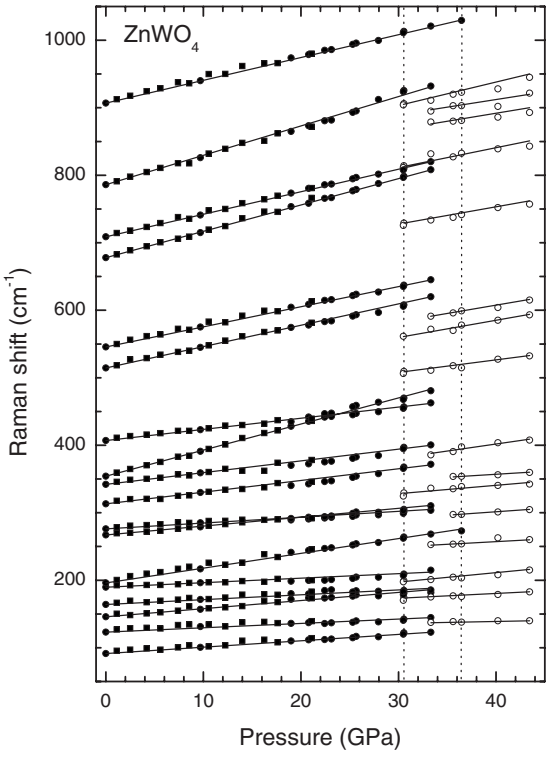

FIG. 3. Pressure dependence of the Raman mode frequencies of the wolframite (solid symbols) and β-fergusonite (empty symbols) phases of $ZnWO_4$. Sample 1: squares and sample 2: circles. The solid lines are just a guide to the eye. The vertical dashed lines indicate the range of coexistence of the wolframite and β-fergusonite phases.

pounds the internal stretching modes are the highest in frequency.[19,20] As we will discuss later this conclusion is also supported by our lattice dynamics calculations.

Recently, the assignment of the internal stretching modes has been obtained in scheelite structured orthotungstates after relating the frequencies (ω) of the stretching W-O modes inside the WO_4 tetrahedra with the Pauling bond strengths (S).[19,20] Using the same approach of Hardcastle and Wachs[50] for tungsten wolframites, we can also obtain the Pauling bond strengths in valence units (v.u.) from the stretching W-O mode frequencies (given in cm^{-1}), which for tungsten oxides is:[19,20]

$$S_{\text{W-O}} = [0.276\ 13\ \ln(25823/\omega)]^{-6}. \quad (1)$$

Thus, it is possible to estimate the formal valence of the W ion in $ZnWO_4$ if we consider all the stretching frequencies of the internal modes of the WO_6 octahedra. By taking, as these frequencies, those we proposed (see Table II) and by considering that the coordination of W in the wolframite structure is 4+2=6, we will get the estimated total valence of 0.442 +0.684+0.969+1.044+1.244+1.598=5.981 (in v.u.) in perfect agreement with the formal valence of the W ion. This fact gives additional support to the assignment of the internal stretching modes we are proposing here. Following the same procedure, we can suggest that the internal stretching modes in wolframite $CdWO_4$ and $NiWO_4$ are at: 900, 775, 710, 690, 550, and 390 cm^{-1} ($CdWO_4$), and 890, 775, 691, 678, 556, and 424 cm^{-1} ($NiWO_4$).

B. Raman measurements of the high-pressure phase

In Fig. 2, it is possible to see that some changes take place in the Raman spectra from 30.6 to 40.2 GPa. First we observed the appearance of eight extra peaks (depicted by ticks in Fig. 2) in addition to the 18 wolframite peaks at 30.6 GPa. In particular, the additional peak located around 900 cm^{-1} is quite strong. At 33.3 GPa new peaks emerge, reaching the total number of 14, while the wolframite peaks can still be clearly observed. It also becomes clear that the strong and broad new peak, located around 900 cm^{-1}, is a triplet. At 36.5 GPa most of the wolframite peaks become very weak and only some of them (e.g., the strongest peak of wolframite located at 1030 cm^{-1} at this pressure) can be observed. At this pressure the new peaks are already 16. At 40.2 GPa, all the wolframite peaks have disappeared and only the 16 new peaks are present. Table III gives the frequencies of the new peaks observed at 40.2 GPa and their pressure coefficients. We think that the changes in the Raman

TABLE III. Frequencies at 40 GPa and pressure coefficients of the Raman modes of the high-pressure phase of $ZnWO_4$. The frequencies and pressure coefficients obtained after *ab initio* calculations are also given. For comparison, the same data form the high-pressure phase of $CdWO_4$ is given at 35 GPa.[31]

Mode	$ZnWO_4$ (40.2 GPa) Raman		$ZnWO_4$ (40 GPa) theory		$CdWO_4$ (35 GPa) Raman	
	ω (cm^{-1})	$d\omega/dP$ (cm^{-1}/GPa)	ω (cm^{-1})	$d\omega/dP$ (cm^{-1}/GPa)	ω (cm^{-1})	$d\omega/dP$ (cm^{-1}/GPa)
A_g	140.1	0.29	141.2	0.04	87	1.4
B_g	179.9	0.72	184.6	0.09	112	0.4
B_g			184.7	0.09	150	0.3
A_g	208.1	1.30	226.2	−0.19	183	0.4
B_g	263.2	0.79	243.4	0.32	213	0.3
B_g			243.5	0.32	240	0.3
A_g	300.1	1.02	293.6	0.93	283	0.5
B_g	339.1	1.24	300.3	0.70	322	1.7
B_g	356.1	0.89	300.4	0.70	378	1.1
A_g	402.1	2.07	375.8	0.97	439	2.7
A_g	527.7	1.86	468.6	2.70	495	0.8
B_g	588.5	2.54	591.4	2.97	572	1.2
B_g	600.9	2.50	591.5	2.97		
A_g	752.7	2.56	715.3	2.74	677	1.7
A_g	839.1	2.92	832.1	2.47	736	2.0
B_g	886.1	2.30	898.1	2.73	768	1.4
B_g	902.1	2.30	898.4	2.75		
A_g	928.0	3.32	906.9	2.54	867	1.7

spectra are caused by the occurrence of a pressure-induced phase transition. The onset of the transition is located at 30.6 GPa and a large coexistence region of both the low-pressure and high-pressure phases is observed between 30.6 and 36.5 GPa. The phase transition is fully completed at 40.2 GPa and is fully reversible with very little hysteresis, as can be seen in the spectrum collected at 0.7 GPa after pressure release. In this spectrum all the observed peaks can be assigned to the 18 Raman modes of wolframite.

Very similar changes to those we observed in $ZnWO_4$ from 30.6 to 40.2 GPa were found by Jayaraman *et al.*[31] in $CdWO_4$ between 20 and 28 GPa. In $CdWO_4$, also 16 modes can be observed in the high-pressure phase, and they are located at similar frequencies as those we detected for the high-pressure phase of $ZnWO_4$. The phonons for the high-pressure phase of both compounds can be compared with the data in Table III. It can be seen that the phonons of $CdWO_4$ resemble those of $ZnWO_4$ but shifted to lower frequencies, in both the high-pressure and low-pressure phases, due to the larger atomic mass of the Cd cation (see Tables II and III and Ref. 31). A similar mass-dependent shift is observed in the Raman spectra of alkaline-earth tungstates following the series: Ba, Sr, and Ca.[19,20] The similitude of the Raman spectra reported by us for $ZnWO_4$ at 40.2 GPa and that reported by Jayaraman for $CdWO_4$ at 35 GPa suggests that the structure of the high-pressure phases of $ZnWO_4$ and $CdWO_4$ can be the same, in a similar way to what is observed in scheelite tungstates.[18–25] A remarkable feature is that the A_g mode that represents the totally symmetric W-O stretching vibration (ω=907 cm^{-1} at ambient pressure and ω=1013 cm^{-1} at 30.6 GPa) in wolframite $ZnWO_4$ drops by about 110 cm^{-1} in $ZnWO_4$ and 120 cm^{-1} in $CdWO_4$ at the phase transition (see Fig. 3 and Ref. 31). This fact suggests that a W-O coordination increase takes place at the phase transition. When the coordination of W increases, the W-O bond lengths usually increase too. The result is a drop in the frequency of the internal stretching modes. This kind of behavior is observed for instance in $Al_2(WO_4)_3$ (Ref. 51) and in the scheelite tungstates[19,20] after a pressure-induced phase transition that imply an increase in the W-O coordination from tetrahedral to octahedral. Another interesting feature observed in the Raman spectra of the high-pressure phases of $ZnWO_4$ and $CdWO_4$ is the appearance of new modes in the phonon gap region of their low-pressure phases (e.g., between 470 and 600 cm^{-1} in ZnWO4 at 30 GPa, see Fig. 3; for $CdWO_4$ see Fig. 2 of Ref. 31). These two facts will be very helpful in identifying the structure of the high-pressure phase of $ZnWO_4$.

Before closing this subsection, we would like to mention that a formation of domains has been observed around 12 GPa in the single crystalline sample (1). This domain formation occurs together with a relative change in the phonon intensity. In particular, the B_g modes—which were much weaker than the A_g modes because of polarization selection rules[52] below 12 GPa—gain in intensity. A similar behavior was described for single crystalline $CdWO_4$ near 10 GPa (Ref. 31) and was interpreted as a phase transition, even though it did not cause any evident change in the Raman

spectra or in the pressure evolution of the phonons. The attribution of the domain formation to structural phase transitions is challenged by the fact that in powder $ZnWO_4$, Perakis *et al.*[32] did not observe any phase transition up to 24 GPa, and we did not observe the onset of it up to 30.6 GPa. A different and more suitable interpretation of this phenomenology could be based on the formation of permanent defects on the sample, as observed recently in optical-absorption measurements in $ZnWO_4$ near 12 GPa.[40] The presence of these defects will cause a breaking of the local structural symmetry producing the increase in the intensity of the B_g modes. The fact that this increase is gradual—and simultaneous with the domain formation—suggests that the domains observed by us in the single crystal of $ZnWO_4$ and by Jayaraman *et al.*[53] in single crystals of $CdWO_4$ are the consequence of the gradual introduction of defects, which can be precursors of the phase transition observed at much higher pressures. Indeed, the introduction of such defects, which leads to a structure with domains separated by antiphase boundaries, was observed in wolframite structured $FeNbO_4$.[54]

Finally, it is well known that in scheelite structured ABX_4 compounds the pressure at which the low-pressure phase becomes unstable is correlated with the BX_4/A radii ratio; the larger this ratio, the higher the transition pressure.[30] Applying the relationship proposed in Ref. 30 to wolframite structured $ZnWO_4$ and $CdWO_4$, we estimate that a pressure-induced phase transition should be expected somewhere beyond 24 and 18 GPa, respectively. These pressures are close to the pressure where the onset of the phase transition is observed in the Raman experiments. This fact supports that only one phase transition is observed in $ZnWO_4$ and $CdWO_4$, being the onset of the transition at 30.6 and 20 GPa, respectively, and the transition completed at 40.2 and 30 GPa, respectively.

C. *Ab initio* calculations

In a recent work, Manjón *et al.*[23] showed experimentally—with the help of *ab initio* calculations—that pressure-induced phase transitions in ABX_4 compounds (in particular in scheelite tungstates and zircons) follow the phenomenological northeast rule in the Bastide diagram. In this sense, we present now the results from our theoretical total-energy calculations of several structural phases of $ZnWO_4$ in order to study the structural stability of the wolframite structure and its possible high-pressure phases. Along with the wolframite structure (SG: $P2/c$),[10] we have considered other structures—paying special attention to phases located to the northeast with respect to wolframite in the Bastide diagram—on account of their observation or postulation in previous high-pressure works for related compounds: $CuWO_4$ type (SG: $P\bar{1}$),[55] orthorhombic disorder wolframite (SG: *Pbcn*),[56] *M* fergusonite (SG: $I2/a$),[57] *M′* fergusonite (SG: $P2_1/c$),[58] $YNbO_4$-type β fergusonite (SG: $C2/c$),[59] monoclinic distorted rutile (SG: $P2/c$),[60] scheelite (SG: $I4_1/a$),[61] $HgWO_4$ type (SG: $C2/c$),[62] *Cmca* (SG: *Cmca*),[18] BaWO4-II type (SG: $P2_1/n$),[63] baddeleyite (SG: $P2_1/c$),[64] and α-$SnWO_4$ (SG: *Pnna*).[65] Figure 4 shows the energy-volume curves for the different structures of $ZnWO_4$, from which the relative stability and coexistence pressures of the phases can be extracted by the common tangent construction.[66] In this figure, we only reported those structures that play a relevant role in the high-pressure structural behavior of $ZnWO_4$. From Fig. 4 it is deduced that the wolframite phase is stable at zero and low pressures up to 39 GPa with an equation of state (EOS), with parameters $V_0 = 137.4$ Å^3, $B_0 = 140$ GPa, and $B_0' = 4.57$ (where the parameters V_0, B_0, and B_0' are the zero pressure volume, bulk modulus, and pressure derivative of the bulk modulus, respectively). These parameters were obtained from our calculations using a third-order Birch-Murnaghan EOS.[67] In the inset of Fig. 4 we show the calculated P-V relationship obtained for wolframite $ZnWO_4$, which corresponds to the above reported EOS. The obtained lattice parameters at ambient pressure compare well with the experimental results with differences within the typical reported systematic errors in DFT-GGA calculations (see Table I). A similar degree of agreement exists for the calculated values of the internal parameters of the wolframite phase.

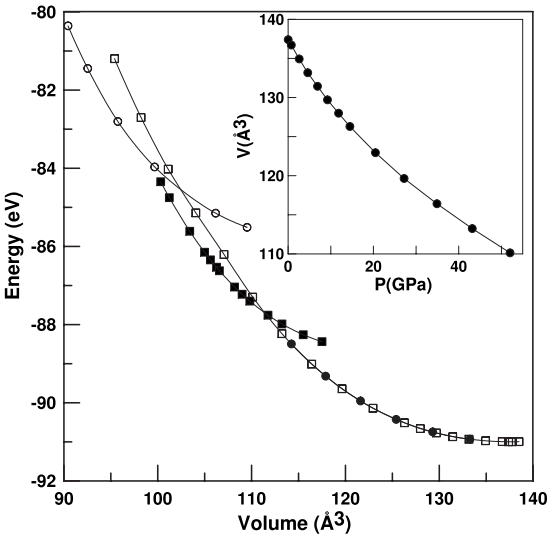

FIG. 4. Energy-volume curves calculated for $ZnWO_4$. Empty squares: wolframite structure; solid circles: $CuWO_4$-type structure; solid squares: β-fergusonite structure; and empty circles: *Cmca* structure. The inset shows the calculated pressure dependence of the volume (symbols) and the obtained equation of state (line) for the wolframite phase.

At low pressures there are three structures in close competition with the wolframite structure: the triclinic $P\bar{1}$, the baddeleyite, and the distorted rutile structures. The triclinic $CuWO_4$-type structure is known to be a metastable phase in wolframite-type $ZnMoO_4$.[68] In $ZnWO_4$, the $CuWO_4$-type structure is expected to become stable at expanded volumes (i.e., *negative* pressures) according to the phase-transition systematics established by Bastide[23,26] based on the ionic radio ratios of the A and B cation and the X anion in ABX_4 compounds. Therefore, it is not strange that this structure is competitive with wolframite. As a matter of fact, the $P2/c$ to $P\bar{1}$ transitions is observed in solid solutions of sanmartinite and cuproscheelite ($CuWO_4$) at around $Zn_{0.78}Cu_{0.22}WO_4$.[69]

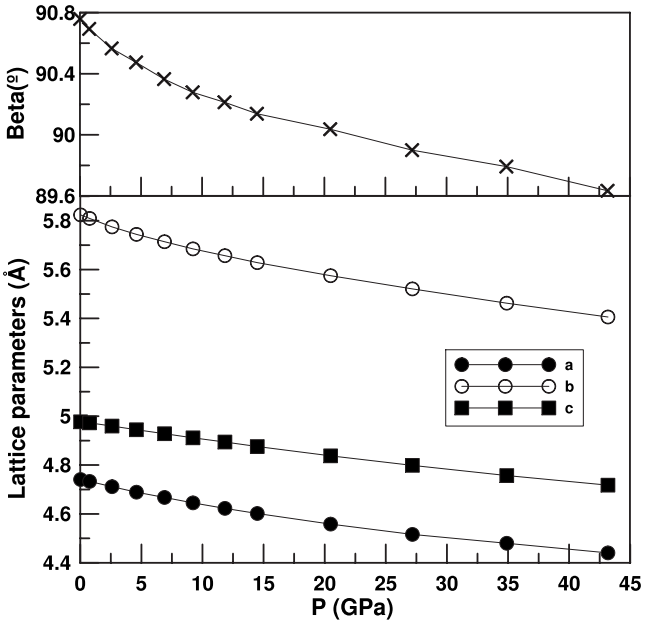

FIG. 5. Theoretically calculated pressure dependence of the lattice parameters and the monoclinic β angle of the wolframite structure of $ZnWO_4$.

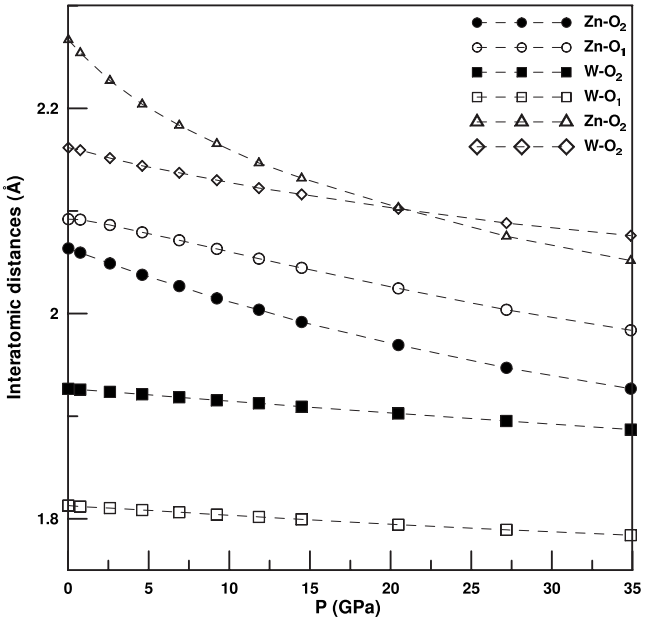

FIG. 6. Theoretically calculated pressure evolution of the Zn-O and W-O interatomic distances in the low-pressure phase of $ZnWO_4$.

This fact suggests that the $P\bar{1}$ to $P2/c$ phase transitions could be observed in $CuWO_4$ upon compression. This picture is consistent with the idea that under pressure the electronic structure of an element of the periodic table becomes similar to that of the next row element, as a consequence of the pressure-induced *sp-d* electron transfer.[70,71] In addition, the group–subgroup relationship existent between the $P\bar{1}$ and $P2/c$ space groups makes the proposed transition quite reasonable from the crystallochemical point of view.[72] On the other hand, the baddeleyite and distorted rutile structures have been also observed as metastable phases in compounds isostructural to $ZnWO_4$, e.g., in $FeNbO_4$.[60] Therefore, it is not strange that these structures are in close competition with the wolframite structure at low pressures.

Figure 5 shows the pressure dependence we obtained from our calculations for the lattice parameters and the monoclinic β angle of wolframite $ZnWO_4$. There, it can be seen that in other orthotungstates the compressibility of $ZnWO_4$ is highly anisotropic. In particular the *c* axis is much less compressible than the other two axes. For example, from ambient pressure to 20 GPa the relative compression of the *a* and *b* axes is approximately 4%, but the relative compression of the *c* axis is only 0.8%. Consequently, the b/c axial ratio decreases considerably upon compression whereas the b/a axial ratio stays nearly constant. A similar behavior has been observed in $CdWO_4$ up to 8 GPa.[47] At the same time, compression also causes a reduction in the β angle. On the other hand, the changes in the atomic positions with pressure are negligible (see Table I). The anisotropic compressibility of wolframite $ZnWO_4$ can be understood in terms of hard anionlike WO_6 octahedra surrounded by charge compensating Zn cations. Figure 6 shows the calculated pressure evolution for the Zn-O and W-O interatomic distances. As can be seen there, there is an important decrease upon compression of the Zn-O bond distances. However the W-O bond distances are nearly uncompressible. In particular, the larger Zn-O bonds are the most compressible bonds, which cause a gradual reduction in the anisotropy of the ZnO_6 octahedra upon compression. A similar uncompressibility of the W-O bonds has been observed in the case of the scheelite structured orthotungstates.[17,18] This means that when pressure is applied the WO_6 units remain essentially undistorted and the reduction in the unit-cell size is basically associated with the compression of the Zn-O octahedral environment. Along the *c* axis the WO_6 units are directly aligned, whereas along the *a* and *b* axes there is a Zn cation between two WO_6 octahedra. Thus, the different arrangement of hard WO_6 octahedra along the *a*, *b*, and *c* axes accounts for the different compressibility of the three unit-cell axes. The uncompressibility of the WO_6 octahedra in wolframite structured orthotungstates, which is similar to that of WO_4 tetrahedra in scheeliite structured orthotungstates, explains why the empirical relation proposed in Ref. 17 for the bulk modulus of scheelite structured AWO_4 compounds also works accurately for wolframite $ZnWO_4$ and $CdWO_4$.

As pressure increases, the wolframite structure becomes unstable against a monoclinic β-fergusonite-type structure. Theoretically, this structure only emerges as a structurally different and thermodynamically stable phase above a compression threshold of about 39 GPa. At the transition pressure the atomic volume of the wolframite phase is 114.89 $Å^3$ (two formula units per unit cell) and the atomic volume of the β-fergusonite phase is 215.54 $Å^3$ (four formula unit per unit cell). Thus the occurrence of the phase transition implies a large volume collapse of about 6%, which suggest that the transition is a first-order reconstructive transformation. The structural parameters obtained for the β-fergusonite structure at 44.1 GPa are given in Table IV and a perspective drawing of it is shown in Fig. 1(b). As can

TABLE IV. Calculated crystal parameters of the β-fergusonite phase of $ZnWO_4$ at 44.1 GPa. Space group $C2/c$, with $Z=4$.

$a=6.814$ Å, $b=9.177$ Å, $c=4.819$ Å, and $\beta=134.976°$				
Atom	Site	x	y	z
Zn	$4e$	0	0.3750	0.25
W	$4e$	0	0.8753	0.25
O_1	$8f$	0.1787	0.7994	0.1222
O_2	$8f$	0.3066	0.9507	0.7355

be seen in the figure, in the high-pressure phase the packing is more compact than in the wolframite structure—being in the β-fergusonite-type structure the W atoms coordinated by four O atoms at 1.84 Å and four additional oxygens at 2.64 Å. On the other hand, in the high-pressure phase the Zn atoms are coordinated by four atoms at a short distance of about 1.95 Å and by four O atoms at a longer distance of about 2.04 Å forming a distorted dodecahedra. This fact implies an increase in the W-O coordination from 4+2 to 4+4, which is in good agreement with the drop of the W-O stretching mode observed at the phase transition. According to our calculation the monoclinic β-fergusonite phase of $ZnWO_4$ remains as the most stable phase up to 57.6 GPa. On further increase in pressure we found that the orthorhombic *Cmca* structure that we proposed in a previous study for $CaWO_4$ and $SrWO_4$ (Ref. 18) becomes favored beyond 57.6 GPa. Unfortunately, our experiments could not be extended up to this pressure in order to check our theoretical prediction. The crystal parameters of the second high-pressure phase are given in Table V and a perspective drawing of it is shown in Fig. 1(c). The most interesting feature of this phase is that it implies a W-O coordination increase from 4+4 to eight and a Zn-O coordination increase from eight to 7+4.

The high-pressure structural sequence we are reporting here (wolframite $\rightarrow \beta$ fergusonite $\rightarrow$ *Cmca*) can be rationalized by means of the phase diagram proposed by Bastide.[23,26] In this diagram the ABX_4 compounds are located according to their cation to anion radii ratios (r_A/r_X, r_B/r_X) and are expected to undergo pressure-induced phase transitions following the northeast rule, i.e., a given compound is expected to take the structure of a compound with larger cation to anion radii ratios. According to this picture, $ZnWO_4$ could probably transform under pressure to the structure of $YNbO_4$ (β-fergusonite) and after that to an orthorhombic *Cmca* structure similar to that of $BaMnF_4$ and $SrUO_4$. Please note that it is possible to transform wolframite into β fergusonite by means of a *klassengleiche* transformation and this structure into *Cmca* by means of *translationengleiche* transformation. Therefore, given the group relationships existent among the three structures, the structural sequence we are proposing here for $ZnWO_4$ is definitely possible on crystallographic grounds. It is important to mention here that the high-pressure β-fergusonite phase of $ZnWO_4$ is closely related from a structural point of view to the high-pressure M-fergusonite phase found in scheelite structured AWO_4 compounds.[17,18] β fergusonite can be obtained by means of symmetry operations from wolframite and M-fergusonite can be obtained by means of symmetry operations from scheelite.[73] Both fergusonite structures are not isostructural but are closely related because both structures are consist of zigzag chains of W polyhedra with eight coordinated A atoms. Apparently, both in wolframite and scheelite structured compounds the fergusonite phases act as a bridge phase between a structure with a low W coordination (such as scheelite and wolframite) and another with high W coordination, such as the *Cmca* structure.

TABLE V. Calculated crystal parameters of the *Cmca* phase of $ZnWO_4$ at 76.1 GPa. Space group *Cmca*, with $Z=8$.

$a=7.1807$ Å, $b=10.3304$ Å, and $c=4.9896$ Å				
Atom	Site	x	y	z
Zn	$8e$	0.75	0.8585	0.75
W	$8f$	0.5	0.3920	0.2590
O_1	$8e$	0.75	0.1741	0.75
O_2	$8f$	0.5	0.2758	0.5444
O_3	$8d$	0.6600	0	0
O_4	$8f$	0.5	0.4217	0.8751

Table II shows the calculated frequencies and pressure coefficients for the Raman modes of wolframite $ZnWO_4$. The agreement between calculations and experiments for the low-pressure phase is quite good, which gives credibility to the lattice dynamics calculations we performed for the high-pressure phase of $ZnWO_4$. It is important to note here that the calculated eigenmodes for wolframite $ZnWO_4$ indicate that there are modes that involve basically a movement of the WO_6 octahedra as rigid units and others that imply internal vibrations of these octahedra. Therefore, despite external and internal modes show similar Grüneisen parameters and this prevents a simple distinction between them, as in scheelite structure compounds, this distinction can be still applied to wolframite structured compounds as we did along the paper. The isolation of the WO_6 octahedra is also evident from the uncompressibility of the W-O already described. According to our lattice dynamic calculations the internal stretching modes are the same that we proposed in Sec. IIA.

Let us know discuss the lattice dynamic calculations performed for the high-pressure phase of $ZnWO_4$. The present Raman measurements are in good agreement with the results obtained from our calculations beyond 39 GPa. In particular, the Raman spectra collected for the first high-pressure phase are best explained for the β-fergusonite structure. Other candidate structure cannot give account for the measured Raman spectra. In the first place, the scheelite structure in tungstates has only 13 Raman-active modes and has a phonon gap from 400 to 700 cm^{-1}.[19,20] So we cannot explain the Raman spectra we observed in the high-pressure phase and therefore is discarded as a candidate structure for the high-pressure phase. In the second place, the M-fergusonite and M'-fergusonite structures in tungstates and the $HgWO_4$ structure have 18 Raman-active modes.[74] However they have their strongest internal stretching mode well beyond 900 cm^{-1}, i.e., as high as those in the scheelite and wolframite phases.[19,20] So these structures cannot explain the drop we observed in the stretching mode basically because they do not imply an increase in

the W-O coordination. In addition, these structures usually also have a phonon gap—which is not present in our Raman spectra. Finally, we have found that the β-fergusonite structure gives a phonon spectrum that can explain reasonably well our experimental results. According to group theoretical considerations the β fergusonite has 18 Raman-active modes at the Γ point: $8A_g+10B_g$. The frequencies and mode assignments of the different phonon calculated for this structure at 40 GPa are given in Table III. According to the calculations there are always two B_g modes very close in frequency to each other, but lattice dynamic calculations apparently tend to underestimate the frequency splitting between B_g modes in fergusonite structures.[19,20] However, the calculated small splitting between B_g modes could explain why in the experiments we have only found 16 modes since some of the B_g modes could be degenerated within the accuracy of the experiments. The qualitative agreement between the calculated and measured phonon frequencies and pressure coefficients is reasonably good. Indeed, among the different structures considered in the calculation, the β-fergusonite structure is the only one that gives a good quantitative agreement with the experiments. In addition, the Raman spectra measured in the β-fergusonite phase of $YNbO_4$ (Ref. 75) resemble very much those measured for the high-pressure phases of $ZnWO_4$ and $CdWO_4$. Therefore, we conclude that we found enough evidence to propose that the high-pressure phase of wolframite structured AWO_4 compounds have a distorted β-fergusonite structure.

V. CONCLUSIONS

We have performed the RT Raman scattering measurements under pressure in $ZnWO_4$ up to 45 GPa. The frequency pressure dependence of all first-order modes of the wolframite phase have been measured up to the completion of the scheelite to β fergusonite phase transitions around 40 GPa. This value of the transition pressure is in good agreement with the estimated transition pressure (39 GPa) according to our *ab initio* total-energy calculations. Our measurements showed that the transition to the β-fergusonite phase starts at 30.6 GPa but is not completed up to 40.2 GPa. The phase transition is reversible and occurs with a volume collapse of about 6%. The *ab initio* calculations also allow us to determine the pressure evolution of the unit-cell parameters of wolframite $ZnWO_4$, being observed that its compression is highly anisotropic. This behavior is related to the different compressibility of Zn-O and W-O bonds, being the last one that is much more rigid than the first one. The calculations also suggest the occurrence of a second pressure-induced phase transition from the β-fergusonite structure to an orthorhombic *Cmca* structure. Additionally, we have performed *ab initio* lattice dynamic calculations for $ZnWO_4$ at selected pressures in the wolframite and β-fergusonite phases. Our calculated mode frequencies in both structures agree with the frequencies of the observed Raman modes and have allowed the assignment and discussion of the nature of the modes.

ACKNOWLEDGMENTS

The authors thank A. Cantarero (ICMUV, Universidad de Valencia) for providing us access to the experimental Raman setup. This work was made possible through the financial support of the MCYT of Spain under Grants No. MAT2007-65990-C03-01, No. MAT2007-65990-C03-03, No. MAT2006-02279, and No. CSD2007-00045, the Generalitat Valenciana under Grants No. ACOMP06/81 and No. GV06/151, and of the Nature Science Foundation of the Fujian Province of China under Grant No. 2005HZ1026. D.E. acknowledges the financial support from the MCYT of Spain through the "Ramon *y* Cajal" program. F.J.M. acknowledges the financial support from "Vicerrectorado de Innovación *y* Desarrollo de la UPV" through Project No. UPV2008-0020. C. Y. T. also acknowledges the support received through the great project of FJIRSM through Project No. SZD08001-2.

*Corresponding author. daniel.errandonea@uv.es

[1] Th. A. Edison, Electr. Eng. **21**, 340 (1896).
[2] W. Chen, Y. Inagawa, T. Omatsu, M. Tateda, N. Takeuchi, and Y. Usuki, Opt. Commun. **194**, 401 (2001).
[3] P. Lecoq, I. Dafinei, E. Auffray, M. Scheegans, M. V. Korzhik, O. V. Missetvich, V. B. Pavlenko, A. A. Fedorov, A. N. Annenkov, V. L. Kostylev, and V. D. Ligun, Nucl. Instrum. Methods Phys. Res. A **365**, 291 (1995).
[4] M. Ishii and M. Kobayashi, Prog. Cryst. Growth Charact. Mater. **23**, 245 (1992).
[5] N. Klassen, S. Shmurak, B. Red'kin, B. Ille, B. Lebeau, P. Lecoq, and M. Schneegans, Nucl. Instrum. Methods Phys. Res. A **486**, 431 (2002).
[6] M. Bravin, M. Bruckmayer, C. Bucci, S. Cooper, S. Giordano, F. von Feilitzsch, J. Hohne, J. Jochum, V. Jorgens, R. Keeling, H. Kraus, M. Loidl, J. Lush, J. Macallister, J. Marchese, O. Meier, P. Meunier, U. Nagel, T. Nussle, F. Probst, Y. Ramachers, H. Sarsa, J. Schnagl, W. Seidel, I. Sergeyev, M. Sisti, L. Stodolsky, S. Uchaikin, and L. Zerle, Astropart. Phys. **12**, 107 (1999).
[7] M. Itoh, N. Fujita, and Y. Inabe, J. Phys. Soc. Jpn. **75**, 084705 (2006); R. Lacomba-Perales, J. Ruiz-Fuertes, D. Errandonea, D. Martinez-Garcia, and A. Segura, EPL **83**, 37002 (2008).
[8] F. A. Danevich, V. V. Kobychev, S. S. Nagorny, D. V. Poda, V. I. Tretyak, S. S. Yurchenko, and Y. G. Zdesenko, Nucl. Instrum. Methods Phys. Res. A **544**, 553 (2005).
[9] A. W. Sleight, Acta Crystallogr., Sect. B: Struct. Crystallogr. Cryst. Chem. **28**, 2899 (1972).
[10] M. Daturi, M. M. Borel, A. Leclaire, L. Savary, G. Costentin, J. C. Lavalley, and B. Raveau, J. Chim. Phys. Phys.-Chim. Biol. **93**, 2043 (1996).
[11] D. Christofilos, S. Ves, and G. A. Kourouklis, Phys. Status Solidi B **198**, 539 (1996).
[12] D. Christofilos, K. Papagelis, S. Ves, G. A. Kourouklis, and C. Raptis, J. Phys.: Condens. Matter **14**, 12641 (2002).
[13] D. Errandonea, M. Somayazulu, and D. Häusermann, Phys. Status Solidi B **231**, R1 (2002).

[14] D. Errandonea, M. Somayazulu, and D. Häusermann, Phys. Status Solidi B **235**, 162 (2003).
[15] V. Panchal, N. Garg, A. K. Chauhan, B. Sangeeta, and S. M. Sharma, Solid State Commun. **130**, 203 (2004).
[16] D. Errandonea, Phys. Status Solidi B **242**, R125 (2005).
[17] D. Errandonea, J. Pellicer-Porres, F. J. Manjón, A. Segura, Ch. Ferrer-Roca, R. S. Kumar, O. Tschauner, P. Rodríguez-Hernández, J. López-Solano, S. Radescu, A. Mujica, A. Muñoz, and G. Aquilanti, Phys. Rev. B **72**, 174106 (2005).
[18] D. Errandonea, J. Pellicer-Porres, F. J. Manjón, A. Segura, Ch. Ferrer-Roca, R. S. Kumar, O. Tschauner, J. López-Solano, P. Rodríguez-Hernández, S. Radescu, A. Mujica, A. Muñoz, and G. Aquilanti, Phys. Rev. B **73**, 224103 (2006).
[19] F. J. Manjón, D. Errandonea, N. Garro, J. Pellicer-Porres, P. Rodríguez-Hernández, S. Radescu, J. López-Solano, A. Mujica, and A. Muñoz, Phys. Rev. B **74**, 144111 (2006).
[20] F. J. Manjón, D. Errandonea, N. Garro, J. Pellicer-Porres, J. López-Solano, P. Rodríguez-Hernández, S. Radescu, A. Mujica, and A. Muñoz, Phys. Rev. B **74**, 144112 (2006).
[21] D. Christofilos, E. Efthimiopoulos, J. Arvanitidis, K. Papagelis, S. Ves, and G. A. Kourouklis, High Press. Res. **26**, 421 (2006).
[22] J. Lopez-Solano, P. Rodríguez-Hernández, S. Radescu, A. Mujica, A. Muñoz, D. Errandonea, F. J. Manjon, J. Pellicer-Porres, N. Garro, A. Segura, Ch. Ferrer-Roca, R. S. Kumar, O. Tschauner, and G. Aquilanti, Phys. Status Solidi B **244**, 325 (2007).
[23] F. J. Manjon, D. Errandonea, J. Lopez-Solano, P. Rodríguez-Hernández, S. Radescu, A. Mujica, A. Muñoz, N. Garro, J. Pellicer-Porres, A. Segura, Ch. Ferrer-Roca, R. S. Kumar, O. Tschauner, and G. Aquilanti, Phys. Status Solidi B **244**, 295 (2007).
[24] D. Errandonea, EPL **77**, 56001 (2007); D. Errandonea, R. S. Kumar, X. Ma, and C. Y. Tu, J. Solid State Chem. **181**, 355 (2008).
[25] D. Errandonea and F. J. Manjón, Prog. Mater. Sci. **53**, 711 (2008).
[26] J. P. Bastide, J. Solid State Chem. **71**, 115 (1987).
[27] D. Errandonea, D. Martínez-García, R. Lacomba-Perales, J. Ruiz-Fuertes, and A. Segura, Appl. Phys. Lett. **89**, 091913 (2006).
[28] D. Errandonea, Chaoyang Tu, Guohua Jia, I. R. Martın, U. R. Rodrıguez-Mendoza, F. Lahoz, M. E. Torres, and V. Lavın, J. Alloys Compd. **451**, 212 (2008).
[29] F. Rivera-Lopez, I. R. Martin, I. Da Silva, C. Gonzalez-Silgo, U. R. Rodriguez-Mendoza, V. Lavin, F. Lahoz, S. M. Diaz-Gonzalez, M. L. Martinez-Sarrion, L. Mestres, and J. Fernandez-Urban, High Press. Res. **26**, 355 (2006).
[30] D. Errandonea, F. J. Manjón, M. Somayazulu, and D. Häusermann, J. Solid State Chem. **177**, 1087 (2004).
[31] A. Jayaraman, S. Y. Wang, and S. K. Sharma, Curr. Sci. **69**, 44 (1995).
[32] A. Perakis, E. Sarantapoulou, and C. Raptis, High Press. Res. **18**, 181 (2000).
[33] J. C. Brice and P. A. C. Whiffin, Br. J. Appl. Phys. **18**, 581 (1967).
[34] P. F. Schofield, K. S. Knight, S. A. T. Redfern, and G. Cressey, Acta Crystallogr., Sect. B: Struct. Sci. **53**, 102 (1997).
[35] R. J. King, Geol. Today **21**, 33 (2005).
[36] D. Errandonea, Y. Meng, M. Somayazulu, and D. Häusermann, Physica B (Amsterdam) **355**, 116 (2005).
[37] D. Errandonea, R. Boehler, S. Japel, M. Mezouar, and L. R. Benedetti, Phys. Rev. B **73**, 092106 (2006).
[38] H.-K. Mao, P. Bell, J. Shaner, and D. Steinberg, J. Appl. Phys. **49**, 3276 (1978).
[39] A. Dewaele, P. Loubeyre, and M. Mezouar, Phys. Rev. B **70**, 094112 (2004).
[40] R. Lacomba-Perales, M.S. thesis, Universitat de Valencia, 2007.
[41] G. Kresse, Computer Code VASP. See: http://cms.mpi.univie.ac.at/vasp
[42] J. P. Perdew, K. Burke, and M. Ernzerhof, Phys. Rev. Lett. **78**, 1396 (1997).
[43] P. E. Blöchl, Phys. Rev. B **50**, 17953 (1994); G. Kresse and D. Joubert, *ibid.* **59**, 1758 (1999).
[44] K. Parlinski, Computer Code PHONON. See: http://wolf.ifj.edu.pl/phonon.
[45] Y. Liu, H. Wang, G. Chen, Y. D. Zhou, B. Y. Gu, and B. Q. Hu, J. Appl. Phys. **64**, 4651 (1988).
[46] H. Wang, F. D. Medina, Y. D. Zhou, and Q. N. Zhang, Phys. Rev. B **45**, 10356 (1992).
[47] J. Macavei and H. Schulz, Z. Kristallogr. **207**, 193 (1993).
[48] P. Tarte and M. Liegeois-Duyckaerts, Spectrochim. Acta, Part A **28**, 2029 (1972).
[49] M. Liegeois-Duyckaerts and P. Tarte, Spectrochim. Acta, Part A **28**, 2037 (1972).
[50] F. D. Hardcastle and I. E. Wachs, J. Raman Spectrosc. **26**, 397 (1995).
[51] N. Garg, V. Panchal, A. K. Tiagi, and S. M. Sharma, J. Solid State Chem. **178**, 998 (2005).
[52] These modes were observed because the polarization is partially lost inside the DAC if the sample is not oriented perfectly parallel to the diamond anvil surface.
[53] F. J. Manjón, D. Errandonea, A. Segura, J. C. Chervin, and V. Muñoz, High Press. Res. **22**, 261 (2002).
[54] R. Theissmann, H. Ehrenberg, H. Weitzel, and H. Fuess, J. Mater. Sci. **37**, 4431 (2002).
[55] L. Kihlborg and E. Gebert, Acta Crystallogr., Sect. B: Struct. Crystallogr. Cryst. Chem. **26**, 1020 (1970).
[56] F. Laves, Acta Crystallogr. **17**, 1476 (1964).
[57] L. N. Kinzhibalo, V. K. Trunov, A. A. Evdokimov, and V. G. Krongauz, Kristallografiya **27**, 43 (1982).
[58] G. M. Wolten, Acta Crystallogr. **23**, 939 (1967).
[59] W. J. Sun, F. J. Ma, and S. J. Zhuang, Sci. Geol. Sinica 1, 78 (1983).
[60] Y. Sugitani, Y. Susuki, and K. Nagashima, Am. Mineral. **70**, 856 (1985).
[61] A. Zalkin and D. H. Templeton, J. Chem. Phys. **40**, 501 (1964).
[62] W. Jeitschko and A. W. Sleight, Acta Crystallogr., Sect. A: Cryst. Phys., Diffr., Theor. Gen. Crystallogr. **A29**, 869 (1973).
[63] I. Kawada, K. Kato, and T. Fujita, Acta Crystallogr., Sect. A: Cryst. Phys., Diffr., Theor. Gen. Crystallogr. **30**, 2069 (1974).
[64] J. D. McCullough and K. N. Trueblood, Acta Crystallogr. **12**, 507 (1959).
[65] W. Jeitschko and A. W. Sleight, Acta Crystallogr., Sect. B: Struct. Crystallogr. Cryst. Chem. **30**, 2088 (1974).
[66] A. Mujica, A. Rubio, A. Muñoz, and R. J. Needs, Rev. Mod. Phys. **75**, 863 (2003).
[67] F. Birch, J. Geophys. Res. **83**, 1257 (1978).
[68] S. C. Abrahams, J. Chem. Phys. **46**, 2052 (1967).
[69] P. F. Schofield and S. A. T. Redfern, J. Phys.: Condens. Matter **4**, 375 (1992).

[70] D. Errandonea, R. Boehler, and M. Ross, Phys. Rev. B **65**, 012108 (2002).
[71] H. L. Skriver, Phys. Rev. B **31**, 1909 (1985).
[72] L. E. Depero and L. Sangaletti, J. Solid State Chem. **129**, 82 (1997).
[73] H. Weitzel and A. Schrocke, Z. Kristallogr. **152**, 69 (1980).
[74] G. Blasse, J. Inorg. Nucl. Chem. **37**, 97 (1975).
[75] N. Tomasic, A. Gajovic, V. Bermanec, D. S. Su, M. Rajic Linaric, T. Ntaflos, and R. Schlogl, Phys. Chem. Miner. **33**, 145 (2006).